MATERIALE PLASTICE
https://revmaterialeplastice.ro
https://doi.org/10.37358/Mat.Plast.1964

Influence of Triangular Pattern Infill on 3D Printed Torus Mechanical Behavior

PATRICIA ISABELA BRAILEANU[1*], DELIA ALEXANDRA PRISECARU[1], NICOLETA CRISAN[2], MARILENA STOICA[1], ANDREI CALIN[1]

[1]Politehnica University of Bucharest, Faculty of Mechanical Engineering and Mechatronics, Department of Machine Parts and Tribology, 313 Splaiul Independentei, 060042, Bucharest, Romania

[2]Politehnica University of Bucharest, Faculty of Industrial Engineering and Robotics, Department of Materials Resistance, 313 Splaiul Independentei, 060042, Bucharest, Romania

Abstract: *The torus or toroidal surfaces are geometries that can be easily found in various industrial applications, from containers, devices, cartwheels, design objects and even machine parts, being also a geometric primitive often used in solid constructive geometry. For a better understanding of the torus–type surface mechanical behavior, this paper aims to study the toroidal geometry manufactured from ABS material by using the FDM 3D printing method and subjecting each sample to compression tests to identify the influence of the sample filling percentage in the case of triangular pattern.*

Keywords: *torus, additive manufacturing, mechanical behavior, compression test*

1. Introduction

The term of torus refers to a geometry generated by the rotation of a circle around an axis placed in its plane, in a three-dimensional space, normally provided that the axis should not intersect the circle, but most of the time, the term is also used for geometries which can be included in the toroidal surfaces category. Although they are not as often remembered, toroidal surfaces are part of countless industrial designs such as the wheels of some trolleys or the surfaces of the worm wheels teeth that show the tips and channels of the teeth inscribed in toroidal surfaces, gaskets used for sealing, furniture components, rings and other, most of the time referring to them in a colloquial way through donut-type surfaces. For this type of torus, the distance from the center of the circle to the center of the torus is greater compared to the radius of the circle ($R_t > r_c$) [1].

If we consider the classical case of torus described in Figure 1a, more precisely a circle rotating around a vertical axis, and the section plane [YZ], the result of this section will be two circles, having both radii equal, in this example 2.5mm [1, 2].

The second particular case of the torus is the horn torus described in Figure 1b, a circle that revolves around a vertical axis, which is tangent to the circle. The result of the section with the [YZ] plane through the torus will be two tangent circles in the frontal plane, with equal radii, as in the previous one. In this case the distance from the center of the circle that rotates around the axis to the center of the torus, denoted by Rt, is equal to the radius of the circle, denoted by r_c ($R_t = r_c$) [1, 2].

And last but not least, the spindle torus, is a special case of the torus shown in Figure 1c, whereby a circle rotates around a vertical axis, which intersects the circle. The result of the section with the [YZ] plane in this case will be two circles of equal radii that intersect, the central part of the torus being a void space. In this sense, the distance from the center of the circle to the center of the torus is less than the radius of the circle rotating around the axis (Rt < rc) [1, 2].

From a parametric point of view, the torus can be defined as follows:

$$x(\alpha, \beta) = (R_t + r_c \cos\alpha)\cos\beta \quad (1)$$

$$y(\alpha, \beta) = (R_t + r_c \cos\alpha)\sin\beta \quad (2)$$

$$z(\alpha, \beta) = r_c \sin\alpha \quad (3)$$

**email: delia.prisecaru@upb.ro*

where:

$\alpha, \beta \in [0,2\pi)$;

α, β - are the angles that determine the formation of a complete circle, implicitly their values start and end in the same point;

R_t - is the distance from the center of the generative circle to the axis, more precisely the center of the torus;

r_c - the radius of the circle that generates the torus.

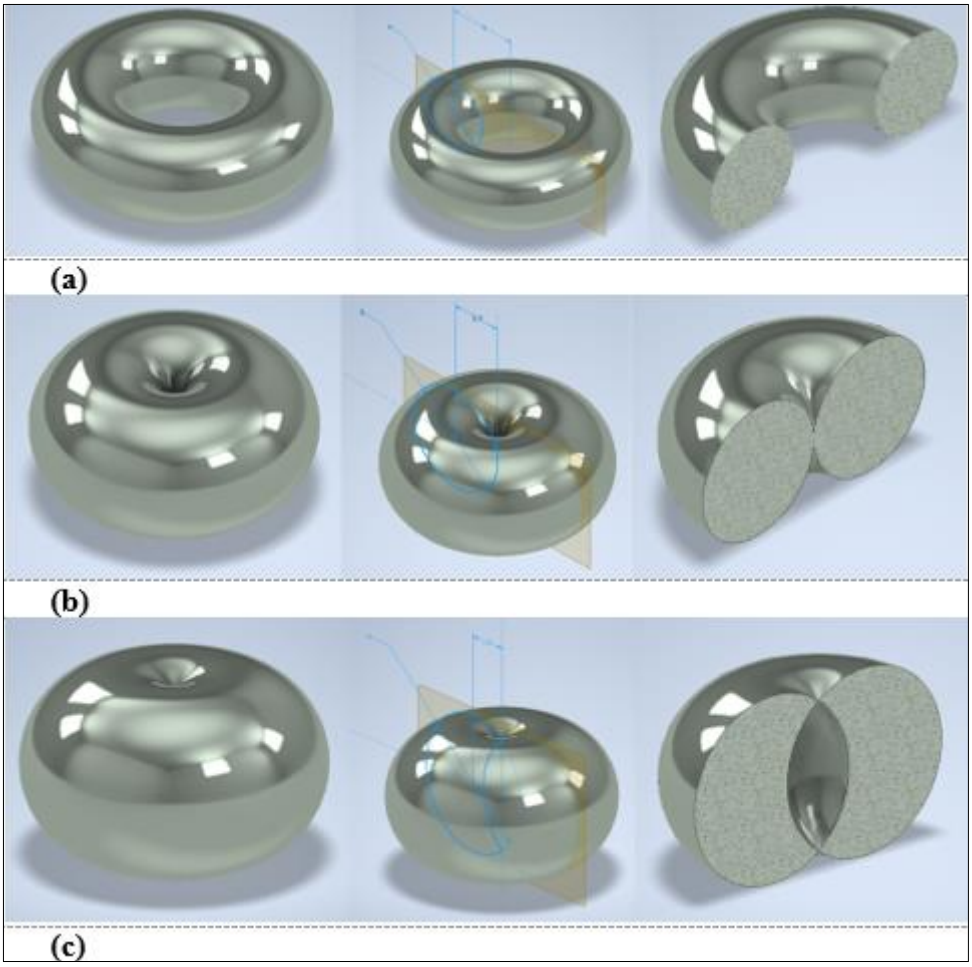

Figure 1. a) Torus regular geometry. Ring torus or anchor torus (R_t>r_c); b) Horn torus (R_t>r_c); c) Spindle torus or self-intersecting torus (R_t>r_c)

Thus, in the case of the anchor ring type torus used in this study, the torus parameters can be determined by using the following values to substitute in the mathematical relationships bellow: R_t=30 mm and r_c=10 mm, where α, β belongs to *[0,2π)* and whence it clearly follows that $R_t > r_c$.

Consequently, the torus equation can be written in the form:

$$\left(x^2 + y^2 + z^2 + {R_t}^2 - {r_c}^2\right)^2 = 4{R_t}^2(x^2 + y^2) \quad (4)$$

The area of the torus [1] can be determined using the following mathematical relation:

$$A = 4\pi^2 R_t \cdot r_c \quad (5)$$

And the volume of the torus [3] or a body bounded by a torus can be deduced by using the following mathematical relation:

$$V = 2\pi^2 R_t \cdot {r_c}^2 \quad (6)$$

Found in various applications related to machine parts as previously mentioned or being integrated as a shape in various designs or assemblies, the term torus can describe both the three-dimensional geometry of a circle that rotates around an axis, as well as a geometry which can be integrated into a torus-type surface, often being confused with toroidal polyhedron, in the latter case the toroid does not need to be circular and can have any number of holes.

2. Materials and methods

This section aims to go through each stage of the study, from the design part of the torus in a dedicated CAD software application, the file import into the software application of the 3D printer in which the model is prepared for additive manufacturing, the printing process chosen with the settings, the materials used in the production of the physical models, the planning method of the samples compression test and the last stage, the actual submission of samples to compression [4].

2.1. Torus design

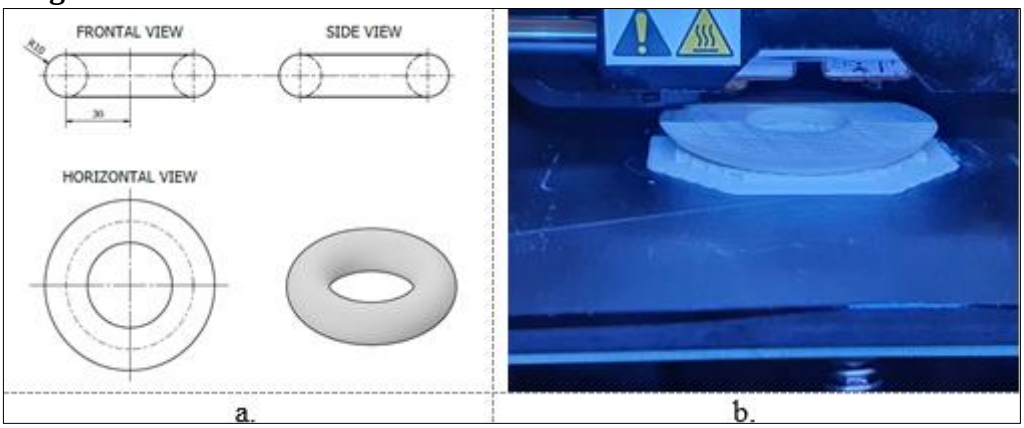

Figure 2. The torus additive manufacturing. a. 3D model of the torus; b. The printing process of a sample

The Autodesk Inventor software application was used to create the three-dimensional solid model of the torus. The sketch of the torus was generated in the *[XY]* plane, in which a circle with a *20 mm* diameter (R_t*=30 mm*, therefore r_c*=10 mm*) was built at *30 mm* from the *XOY* coordinate system center, and from the *XOY* origin system, a construction axis coincident with *OY* was drawn. After the sketch was completed, the revolve tool was used to rotate the circle around the construction axis. Afterwards, the file was exported to a **.stl* file extension (stereolithography) to be imported into FlashPrint 3D software application.

Figure 2a shows the dimensions used in the torus design as a technical drawing form, in which we can visualize all three of its projections (vertical, horizontal, lateral projection and an isometric projection of the 3D model).

2.2. The material used in torus manufacturing

PRIMAVALUE ™ is a high-quality filament, an ABS (*Acrylonitrile Butadiene Styrene*) type material used in 3D printers that use the FDM (*Fusion Deposition Material*) method [5] and which lends itself to the generation of printable prototypes of any type, for everyday use [6 - 8] with a printing filament diameter of *1.75 mm*, tolerance *±0.05 mm* and *≥ 95 %* roundness.

The material has good mechanical properties, shows high strength and withstands temperature fluctuations, has good interlayer adhesion and toughness. The general physical and thermal properties [9] are described in Table 1.

Table 1. The general properties of PRIMAVALUE ™ ABS [7]

Type	Properties	Value	US	Test Method
Physical	Relative Density	1,03	g/cc	ASTM D792
	Tensile strength	44	MPa	ISO 527
	Tensile modulus	2000		ASTM D638
	MFR 220°C/10 kg	8,0	g/10 min	ASTM D1238
	Impact strength Izod method 23°C	36	KJ/m^2	ISO 180/A
Thermal	Melting Temperature	220 – 270	°C	ISO 294
	Printing Temperature	245 ±10		–
	Vicat softening Temperature	±103		ISO 306

2.3. Torus samples manufacturing process

The model preparation for printing was carried out in the FlashPrint software application created especially for the *FlashForge Creator Pro* 3D printers that were used in the manufacture of the samples used.

In this study, 10 samples with identical geometric features were generated, being manufactured by using the FDM method with the same material mentioned previously. The printer's settings coincide for all geometric models, the only difference being the sample filling percentage.

The **.stl* file generated in the previous step in *Autodesk Inventor* was imported into the FlashPrint application, where it was centered on its platform and set in contact with it. The printing process for each sample was performed with a single extruder, specifically the right extruder, using a support and a linear raft for the geometry to facilitate detaching the model from the 3D printer platform when the process is complete, in this way the sample surface damage is reduced as much as possible.

Thus, the following print settings were used: 0.12 mm for the layer height; 0.2 mm for the first layer height; 3 perimeter shells; 4 top solid layers and bottom solid layers; 50 mm/s print speed; 70 mm/s travel speed; 230°C the temperature for the right extruder, and 90°C the platform temperature. For the infill settings [10, 11], a triangle pattern was used, and the fill percentage starts from 10% for the first torus sample and continues from 10 to 10, until it reaches the last sample with a filling percentage of 100%.

Table 2 shows the sample data and the estimated values by the software application FlashPrint before the printing process.

Table 2. The torus samples data an estimated value from FlashPrint software

Sample n°	Fill percentage [%]	Estimated filament length [m]	Estimated weight [g]	Estimated printing time
1	10	5.76	14.4	1 h 20 min.
2	20	7.52	18.82	1 h 41 min.
3	30	9.21	23.04	2 h 1 min.
4	40	10.91	27.3	2 h 21 min.
5	50	12.65	31.63	2 h 40 min.
6	60	14.34	35.88	2 h 59 min.
7	70	16.03	40.09	3 h 18 min.
8	80	17.74	44.38	3 h 36 min.
9	90	19.45	48.65	3 h 53 min.
10	100	19	47.53	3 h 24 min.

After the printing stage, all the samples were checked again, the length of the filament used for printing each sample according to the filling percentage, the actual printing time and each sample was also weighed with a high-precision Ohaus Pioneer Laboratory Balance, the results been listed in Table 3.

A slight discrepancy can be observed between the printing time proposed by the 3D printer software application and its actual printing time, the last one being smaller. The length of the filament proposed for each sample by *Flash Print* is very similar to the one obtained after printing, in some places slightly exceeding the amount of filament proposed by the application or even being coincidental, as in the case of *sample number 4*.

Table 3. The data results after 3D printing the samples with FlashForge Creator Pro

Sample n°	Fill percentage [%]	Filament length used [m]	Effective samples weight, [g]	Effective printing time
1	10	5.7575	10.1444	1 h 17 min
2	20	7.5257	13.7894	1 h 36 min
3	30	9.2112	17.5035	1 h 55 min
4	40	10,910	21.0885	2 h 14 min
5	50	12,644	24.7482	2 h 32 min
6	60	14,342	28.2713	2 h 49 min
7	70	16,022	31.7722	3 h 7 min
8	80	17,740	35.0725	3 h 16 min
9	90	19,440	37.9196	3 h 40 min
10	100	18,996	38.3964	3 h 14 min

2.4. Torus compression test

The compression test was carried out with Istron® 8872 testing system, an equipment suitable for carrying out fatigue and static tests for parts made of different materials and belonging to different industrial fields. Due to revolved shape that the torus has, the design and manufacturing of two PLA supports [12, 13], which will have the role of maintaining the vertical position of the torus, preventing the piece sliding on the surface of the equipment, was carried out (Figure 3).

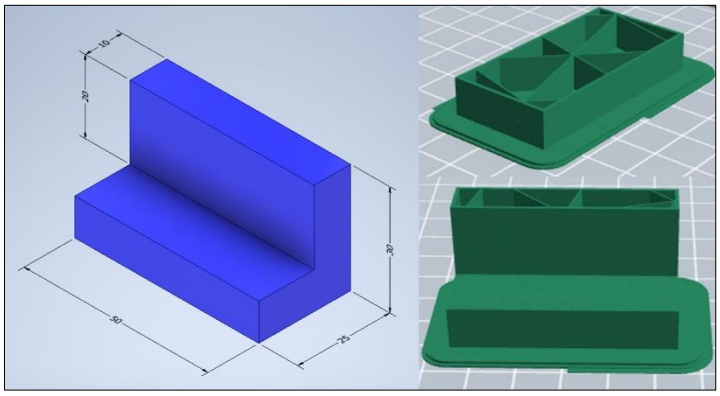

Figure 3. Torus fixing supports used in the compression test

Before the test was initiated the torus was placed in a vertical position on the equipment platform surface and centered, then the two supports were placed on one side of the sample and the other to maintain it in a vertical position. Also, the supports were fixed to the equipment platform with paper tape as shown in Figure 4. A plastic film was placed around the test area to prevent the dispersion of sample residues in the event of its breakage during the compression test. The upper grip fixture travel speed was set to 1 mm/min from the software application to which the test equipment is connected.

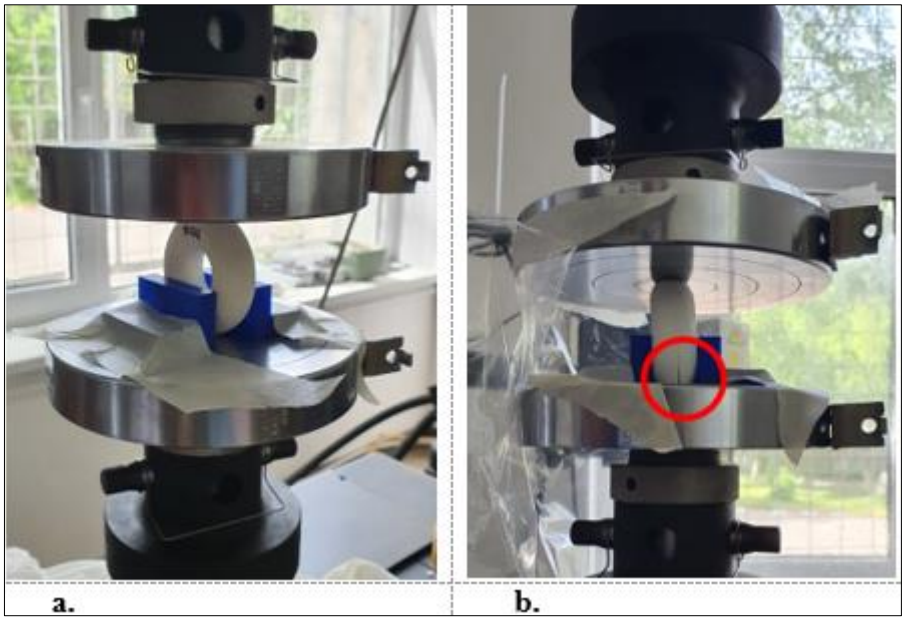

Figure 4. Sample compression test. a. Positioning the sample for the compression test; b. Cracks appeared in the sample after test completion

3. Results and discussions

The general results obtained for all samples can be seen in Figure 5, where the graph of the compression test evolution and the failure moment of each individual sample is presented. Concerning the sample with a filling percentage of 10%, can be observed the failure of the outer walls shown in Figure 4b. around the force of ~374 N. The sample with a filling percentage of 20% starts to lose its stability what generates the appearance of the buckling phenomenon around ~840 N, the one with a filling percentage of 30% loses its stability at a force of ~1745 N, the sample with a percentage of 40% filling starts to buckle and fails at approximately 2438 N, at the sample with a percentage of 50% filling the bending phenomenon on the curved bar appears and fails at approximately 3435 N, the sample with a fill of 60% fail at ~4040 N, the one with a filling percentage of 70% fail at ~4600 N, the sample with 80% fill fail at ~5180 N, the sample with a filling percentage of 90% fail at approximately 5835 N and last but not least the sample with 100% filling of the torus shape fails at approximately 7000 N.

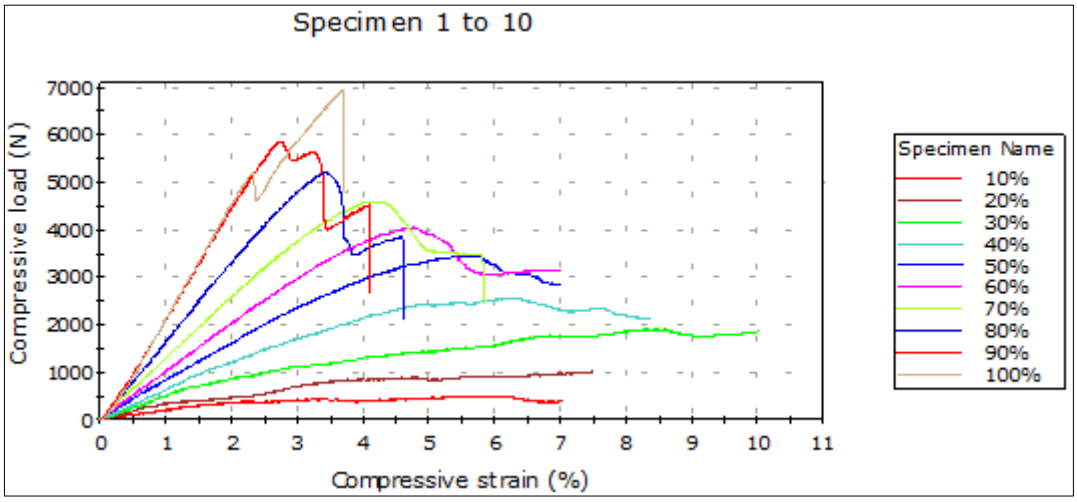

Figure 5. The compression test graph evolution

After compression tests, all samples were sectioned in half and then analyzed both globally (Figure 7) and under a microscope (*NIKON SMZ 1000*) to observe the inside structure damage for each sample

(Figure 8). For reference, in Figure 6 the geometrical pattern is shown before the compression test was initiated.

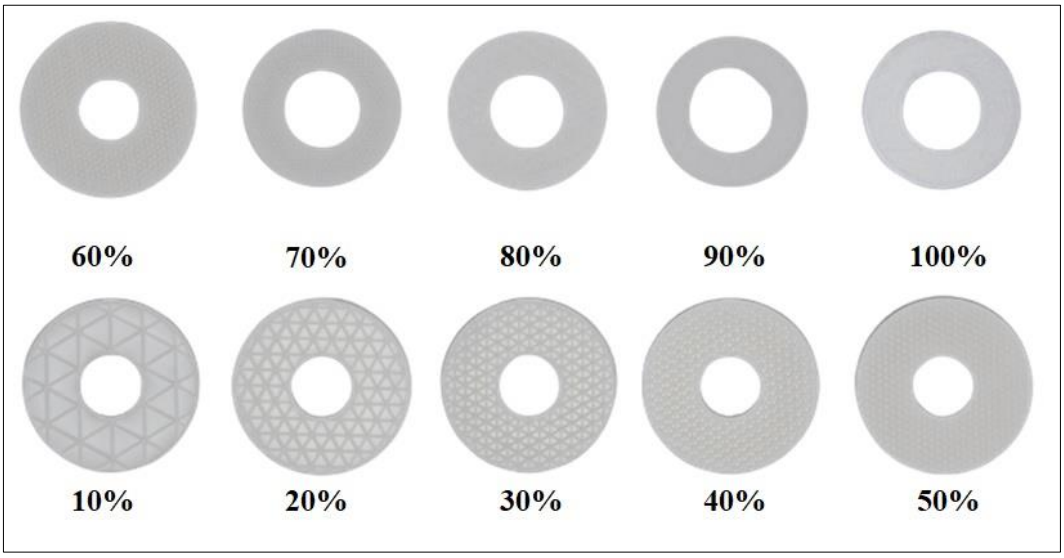

Figure 6. Samples sections before the compression test

The characteristic curve obtained for samples with 10, 30, 50% infill, indicates the presence of considerable plastic deformations before the fracture occurs. The sample with 90% infill can withstand higher loads but its mechanical behavior is similar to the one exhibited by fragile materials.

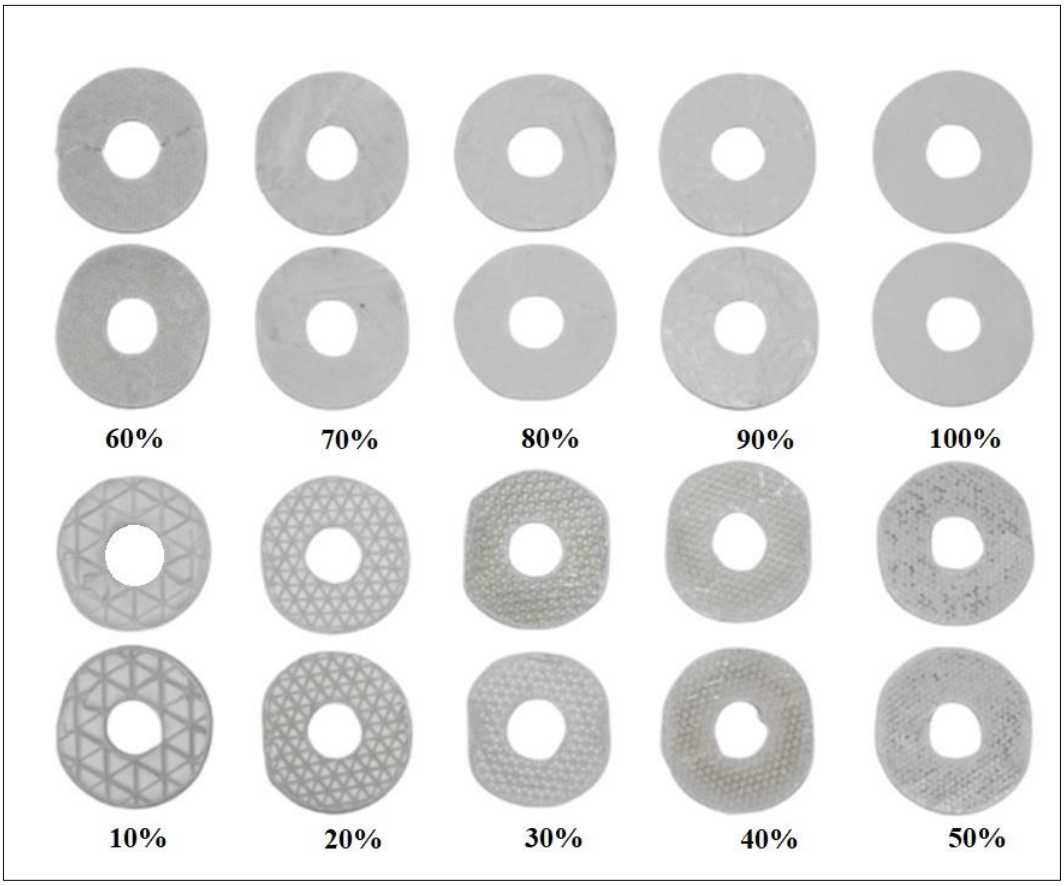

Figure 7. Samples sections after the compression test

Eaven if the sample with 90% fill withstand higher loads it will be preferred to use the one with 50% infill due to its ductile mechanical behavior.

Observing the samples at macrolevel, as shown in Figure 6, validates the printing process was performed without structural errors. Figure 7 shows the internal structure at microlevel of the printed samples after compression tests. Due to the smaller percentage infill, the gaps in the structure allow more deformations. Even if a small brim brakes, the whole structure resists. This can be observed better for 50% infill. As the infill percentage increases, the damaged area, at microstructure level, is less visible.

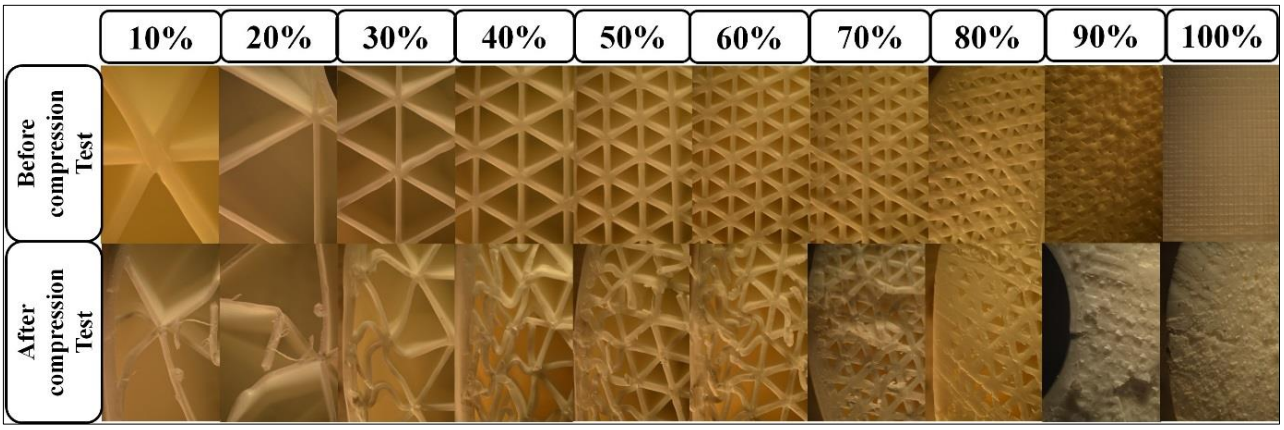

Figure 8. Microscopic analysis of the samples before and after the compression test

A graphical representation based on the estimated weight and effective weight of the samples can be observed in Figure 9a. The estimated value for weight from FlashPrint software is higher with almost 25% than the effective value measured after printing.

Concerning the effective printing time (Figure 9b), the FlashForge Creator Pro software reveals that the effective total printing time it was smaller with 6%, that estimated.

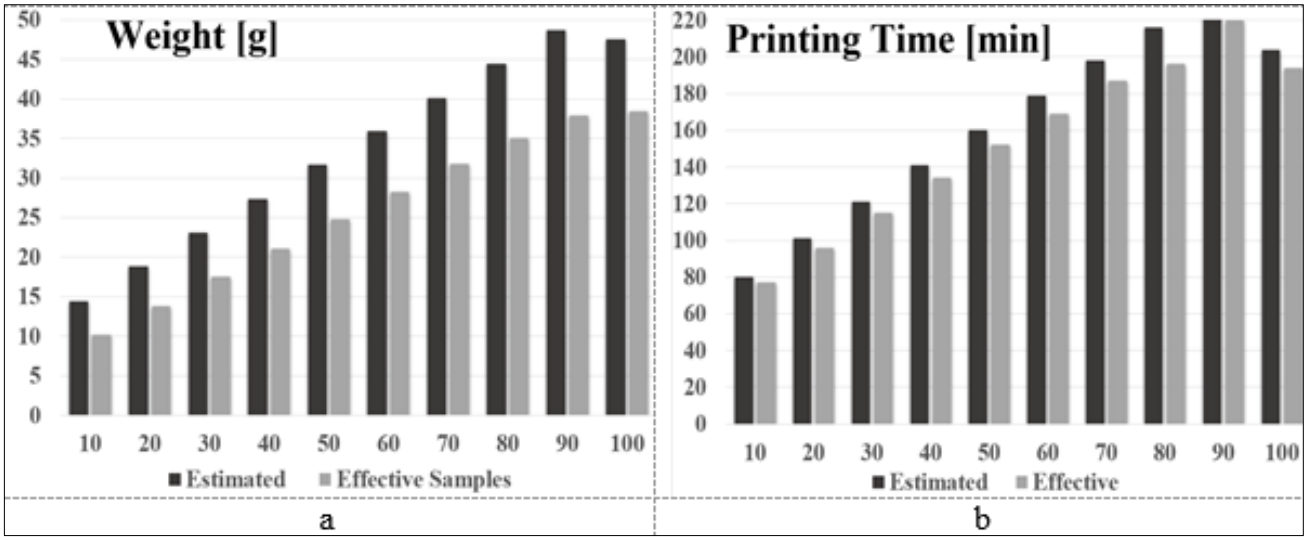

Figure 9. Comparative values a) weight; b) printing time

4. Conclusions

Despite their infrequent mention, toroidal surfaces are a common element of industrial designs, such as the wheels of some trolleys, the surfaces of teeth inscribed in worm wheels, gaskets, furniture components, rings, and many other things, usually referred to in colloquial terms through donut-shaped surfaces. In this paper, the mechanical behaviour of 3D printed samples from ABS material, based on a toroidal geometry was studied.

From different types of toroidal geometry, the classical one was chosen to be the test subject for the influence of triangular pattern infill on the structure's mechanical behaviour.

The infill percentage used to manufacture the samples started at 10% and gradually increased by 10 to 100%. All these samples were subjected to compression tests with a maximum load of 7000 N. Only the sample with 100% infill withstood to the maximum load applied.

Although the maximum load was achieved at 100%, this was not the case for the rest of the infill percentage. So, the infill percentage is not proportional to the supported load, it doesn't increase gradually.

There are significant plastic deformations present before the fracture, according to the characteristic curve derived for samples with 10, 30 and 50% infill. The sample with 90% infill is capable of withstanding greater stresses, but its mechanical behaviour is comparable to that of fragile materials. It is recommended to use the sample with 50% infill due to its ductile mechanical behaviour even though the sample with 90% fill may tolerate larger loads.

This paper represents the starting point in studying new materials and new fabrication method for the existing rollers for trolleys or roller skates. Thus, future work will include studying the tribological behaviour of samples with toroidal geometry.

References

1.WEISSTEIN, ERIC W., Torus, https://mathworld.wolfram.com/Torus.html, accessed on March 10, 2021.
2.PRECUPETU, P., DALE, C., Descriptive geometry exercises with technical applications (Probleme de geometrie descriptivă cu aplicații în tehnică, Editura Tehnica, Bucharest, 1987, 155-159.
3.FARMER, J., The volume of a torus using cylindrical and spherical coordinates, Australian Senior Mathematics Journal, **19**(2), January 2005, 49-58.
4.NAJMON J.C., RAEISI S., TOVAR A., Review of additive manufacturing technologies and applications in the aerospace industry, *Additive Manufacturing for the Aerospace Industry*, 2019, 7-31, https://doi.org/10.1016/B978-0-12-814062-8.00002-9.
5.ALIONTE, C. G., UNGUREANU, L. M., ALEXANDRU, T. M., Innovation Process for Optical Face Scanner Used to Customize 3D Printed Spectacles, **15**(10), Article number 349, 2022, https://doi.org/10.3390/ma15103496.
6.PASCU, N.E., DOBRESCU, T.G., BALAN, E., JIGA, G., ADIR, V., Design of ABS Plastic Components through FDM Process for the Quick Replacement of Outworn Parts in a Technological Flow, *Mater. Plast.*, **55**(2), 2018, 211-214. https://doi.org/10.37358/MP.18.2.4997.
7.*** PRIMAVALUE™ ABS Technical Data Sheet, available at www.primacreator.com/products/, accessed on May 12, 2021.
8.VLASCEANU, D., BACIU, F., POPESCU, D, HADAR, A., MARINESCU, R., Development and 3D Printing of an ABS Ergonomic Handle for Medical Use A case study, 2018, **55**(4), 630-633, https://doi.org/10.37358/MP.18.4.5090.
9.TYMRAK, B.M., KREIGER, M., PEARCE, J.M., Mechanical properties of components fabricated with open-source 3-D printers under realistic environmental conditions, *Materials&Design*, **58**, June 2014, 242-246. https://doi.org/10.1016/j.matdes.2014.02.038.
10.VOICU, A., D., HADAR, A., VLĂSCEANU, D., Benefits of 3D printing technologies for aerospace lattice structures, Scientific Bulletin of Naval Academy, **XXIV**, 2021, 8-16, https://doi.org/10.21279/1454-864X-21-I1-001.
11.DAMINABO, S.C., GOEL, S., GRAMMATIKOS, S.A., NEZHAD, H.Y., THAKUR, V.K., Fused deposition modeling-based additive manufacturing (3D printing): techniques for polymer material systems, *Materials Today Chemistry*, **16**, 2020, 100248, https://doi.org/10.1016/j.mtchem.2020.100248.

12.ZHUO, X., RAKEL, F., SEYED, M., JAVAD, R., Thickness effect on the mechanical behavior of PLA specimens fabricated via Fused Deposition Modeling, *Procedia Structural Integrity*, **33**, 2021, 571-577, https://doi.org/10.1016/j.prostr.2021.10.063.
13.CHISIU, G., STOICA, N., A., STOICA, A., M., Friction Behavior of 3D-printed Polymeric Materials Used in Sliding Systems, *Mater. Plast.*, **58**(1), 2021, 176-185, https://doi.org/10.37358/MP.21.1.5457.

Manuscript received: 25.10.2022